Scanning Microscopy

Volume 9 | Number 1 Article 2

12-23-1994

Ionoluminescence: A New Tool for Nuclear Microprobes in Geology

C. Yang
Lund University and Institute of Technology

N. P. -O. Homman
Lund University and Institute of Technology

K. G. Malmqvist
Lund University and Institute of Technology

L. Johansson
Institute of Geology, Solvegatan

N. M. Halden
University of Manitoba

See next page for additional authors

Ionoluminescence: A New Tool for Nuclear Microprobes in Geology

Authors

C. Yang, N. P. -O. Homman, K. G. Malmqvist, L. Johansson, N. M. Halden, and V. Barbin

Scanning Microscopy, Vol. 9, No. 1, 1995 (Pages 43-62) 0891-7035/95$5.00+.25
Scanning Microscopy International, Chicago (AMF O'Hare), IL 60666 USA

IONOLUMINESCENCE: A NEW TOOL FOR NUCLEAR MICROPROBES IN GEOLOGY

C. Yang[1*], N.P.-O. Homman[1], K.G. Malmqvist[1], L. Johansson[2], N.M. Halden[3], and V. Barbin[4]

[1]Dept. Nuclear Physics, Lund University and Institute of Technology, Sölvegatan 14, S-223 62 Lund, Sweden
[2]Department of Mineralogy and Petrology, Institute of Geology, Sölvegatan 13, S-223 62 Lund, Sweden
[3]Department of Geological Sciences, University of Manitoba, Winnipeg, Manitoba, R3T 2N2, Canada
[4]Univ. Reims Champagne-Ardenne, Faculte des Sciences, Lab. Sciences de la Terre, 51062 Reims Cedex, France

(Received for publication April 11, 1994 and in revised form December 23, 1994)

Abstract

When an ion beam in the energy range of a few MeV/amu impacts on a mineral, visible light can often be observed. This light, induced by energetic ions, is termed ionoluminescence (IL). The intensity and wavelength of the ionoluminescent light provide information concerning the nature of luminescence centers, such as trace substituents and structural defects, found in the mineral. This makes IL a useful complement to other methods of ion beam analysis (IBA), such as particle induced X-ray emission (PIXE) and Rutherford backscattering (RBS), in characterizing geological samples. In the present study, a proton or alpha particle beam was used for the IL excitation and IBA with a nuclear microprobe. The results obtained with IL were compared with those of cathodoluminescence (CL) and photoluminescence (PL).

Key words: Ionoluminescence, cathodoluminescence, photoluminescence, ion beam analysis, particle induced X-ray emission (PIXE), luminescence centers, trace substituents, structural defects, nuclear microprobe.

*Address for correspondence:
Changyi Yang
Department of Nuclear Physics,
Lund University and Institute of Technology
Sölvegatan 14, S-223 62 Lund,
Sweden

Telephone number: +46+46-10 77 41
FAX number: +46+46-10 47 09

Introduction

Figure 1 (modified from Malmqvist, 1991) shows different types of radiation emitted simultaneously in the vicinity of the target point when a beam of energetic particles interacts with a target material. Some of these can be used for the chemical or surface characterization of a variety of materials. For example, particle induced X-ray emission (PIXE) is a very well established method frequently used for quantitative trace element analysis (Johansson and Campbell, 1988). Another method, Rutherford backscattering (RBS), is widely employed for the characterization of surface structure, yielding high depth resolution (Chu *et al.*, 1978). Still another method, nuclear reaction analysis (NRA), can be used for analysis of light elements (Feldman and Picraux, 1977; Demortier, 1992).

However, the routine ion beam analysis (IBA) methods just referred to are quite insensitive to the chemical surroundings of an element and its chemical valence state, since the interaction physics involved in the signal production process occurs for PIXE within the core electron shells and for RBS and NRA within the nucleus. Important chemical information concerning ion valence, local crystal structure, chemical bonding and the like, is not accessible with these techniques. A useful technique for obtaining such information is that of ionoluminescence (IL), a method based on the general characteristics of luminescence. IL is produced when an ion beam in the energy range of a few MeV/amu impacts on a mineral. The IL spectrum (intensity and wavelength) generated by luminescence centers in the mineral yields information concerning trace substituents and structural defects. This makes IL a useful complement to other IBA methods (Ryan, 1993; Swietlicki *et al.*, 1993; Yang *et al.*, 1993, 1994; Bettiol *et al.*, 1994). The additional chemical information that IL method provides can be important in various applications. Thus, IL can be used to determine oxidizing or reducing conditions of mineral growth, for example, by using the IL ratio of Eu^{3+}/Eu^{2+} in such minerals as apatite and feldspar to obtain information concerning oxygen fugacity.

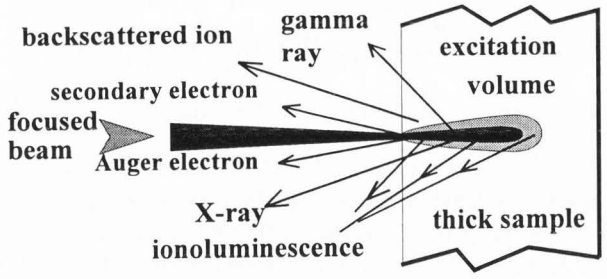

Figure 1. Various types of radiation emission from the interaction between an ion beam and a thick sample (modified from Malmqvist, 1991).

Cathodoluminescence (CL) is a method closely analogous to IL and has been widely employed in geological applications (Kearsley and Wright, 1988; Marshall, 1988; Remond *et al.*, 1992). Another, highly traditional method is that of photoluminescence (PL).

Luminescence can be divided into two types, intrinsic and extrinsic, according to their origin. The intrinsic luminescence, which usually contributes to emission through crystal structural defects, is not related to impurities, but to crystal lattice properties; while the extrinsic luminescence is dependent on the roles of impurities in a crystal through such effects as luminescence activation, sensitization, and quenching. PIXE is a sensitive analytical technique for trace element analysis with the capability of quantification and low detection limit. Therefore, the combination of PIXE and IL offers an effective way of directly relating impurities to the extrinsic luminescence phenomenon. A special emphasis in this paper is given to the extrinsic type IL.

The IL work is still at an early stage. The major feature of the data presented here is qualitative, similar to CL in geological work. The main purpose of this introductory paper is to demonstrate that IL is a complementary technique to other IBA methods, and that the combination of IL and IBA techniques can offer a new tool for a general luminescence study in geology. An improvement toward quantitative IL results may be expected when the details of luminescence physics concerning IL production in multi-impurity systems involved (in quantifying the processes of luminescence activation, sensitization and quenching) can be made clear, and the IL data processing software can be established.

Mechanism of Luminescence in Solids

Luminescence phenomena are common in many solids, yet extensive use of the light produced is restricted because of the complicated physics underlying its emission. For insulators, to which many minerals belong, crystal field theory can be used to explain luminescence (Henderson and Imbusch, 1989), whereas for semiconductor crystals, band theory is often employed (Yacobi and Holt, 1990).

Luminescence with different excitation sources

A great variety of materials luminesce when excited with photons, X-rays, electrons, protons or alpha particles. Pringsheim (1949), Leverenz (1950), and Derham *et al.* (1964) have shown that the general luminescence properties of a material are not dependent on the nature of the excitation source. This holds true as long as no secondary effects such as lattice damage or crystal modification occurs.

For excitation by energetic particles, the process leading to luminescence tends to take place in three stages. In the first stage, excitation energy is absorbed to form an optical excitation volume. Interaction between particles of the incident beam and the material produces secondary emissions such as X-rays, secondary electrons and recoiled atoms. The energy of the secondary particles is converted to ionization energy by an ionization process. Recombination of the electrons and the excited ions allows the crystal lattice to absorb the released energy, as a result, the optical system becomes highly excited. The second stage involves the de-excitation of the states of high excitation through radiation-less transition. In the third stage, luminescence emission occurs when the atoms de-excite from a low excitation state to the ground level. Details of the energy levels in the band gap involved can be investigated through absorption and excitation spectra using photons. In luminescence spectra, however, only one or a few of the lowest levels excited show up in the emission spectra.

Data on photon absorption, excitation and luminescence emission (Dieke and Crosswhite, 1963; Dieke, 1968; Marfunin, 1979; Henderson and Imbusch, 1989) are of use in the study of IL. When IL results are compared with those of PL, the differences between IL and PL become evident. In PL, for example, ionization processes may not necessarily be involved in the selective excitation that occurs, and the energy levels of excitation that can be achieved are not as high as they are for the IL and CL mode. Hence, the ratio of energy conversion to luminescence emission levels, and consequently the relative intensities of different luminescence emissions, can be quite different from those of IL and CL.

Energy levels and luminescence transitions in transition metal ions

Transition metal ions, with an electron configuration of $3d^{(1-9)}$, can interact strongly with a crystal field, resulting in changes in the free ion's energy level structure. Usually, the luminescence activated by transition metal ions $3d^{(1-9)}$ is characterized by a broad peak

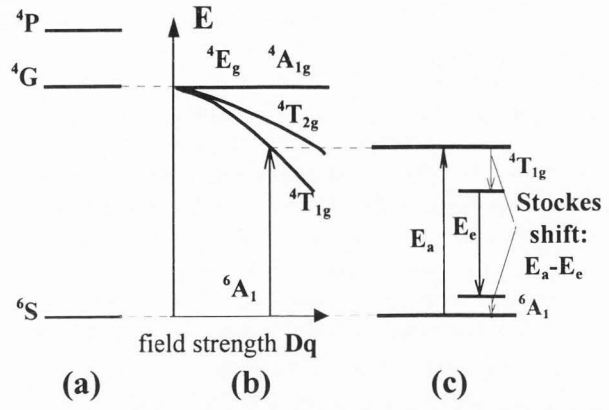

Figure 2. The energy level features of Mn^{2+} and the luminescence transition: (**a**) free Mn^{2+}; (**b**) energy levels as modified by a crystal field; (**c**) Stokes shift in luminescence emission (modified from Marfunin, 1979).

---

width, a large Stokes shift, and a changeable peak position dependent upon the host matrix. The center and width of the peak are very sensitive to the chemical surroundings in the crystal and may be used to distinguish the host matrices involved. For example, if $Mn^{2+}(3d^5)$ ions are located in a crystal having a stronger crystal field, the luminescence produced tends to be of longer wavelength. The luminescence of Mn^{2+} activated calcite (Mn^{2+} ions in octahedral coordination), for example, is orange, whereas the luminescence of Mn^{2+} activated willemite (Mn^{2+} ions in tetrahedral coordination) is greenish (Marfunin, 1979).

The structure of the Mn^{2+} energy levels and of the emission transition is shown in Figure 2. Through the interaction of the Mn^{2+} ions with the crystal field (as described in terms of field strength Dq), the energy level ^4G of the free Mn^{2+} ions is split into separate levels designated as $^4T_{1g}$, $^4T_{2g}$, ^4E_g and $^4A_{1g}$. These energy levels are a function of the field strength Dq of the crystal (Fig. 2b). The luminescence emission occurs at the level $^4T_{1g}$, and there is a Stokes shift in the emission spectrum.

Luminescence characteristics of rare-earth element (REE) ions

Dieke and Crosswhite (1963) have made a comprehensive investigation of all energy levels of REE^{3+} and REE^{2+} ions, expressing their results in the Dieke diagram (Dieke and Crosswhite, 1963), which can be a helpful guide for the IL studies of the REE ions.

The electron configurations of neutral REE atoms in the ground state is REE^0: $4f^{(n)}[5s^25p^6]$-$[6s^2]$, with the three exceptions of Ce^0: $4f^1[5s^25p^6]$ $\underline{5d}^1$ $[6s^2]$; Gd^0: $4f^7[5s^25p^6]$ $\underline{5d}^1$ $[6s^2]$; and Lu^0: $4f^{14}[5s^25p^6]$ $\underline{5d}^1$ $[6s^2]$. For divalent REE ions in the ground state, the general electron configuration is REE^{2+}: $4f^{(n)}[5s^25p^6]$, with the three exceptions of Ce^{2+}: $4f^1[5s^25p^6]$ $\underline{5d}^1$; Gd^{2+}: $4f^7[5s^25p^6]$ $\underline{5d}^1$; and Lu^{2+}: $4f^{14}[5s^25p^6]$ $\underline{5d}^1$, whereas for all trivalent REE ions in the ground state the electron configuration is REE^{3+}: $4f^{(n-1)}[5s^25p^6]$. Trivalent REE^{3+} and most divalent REE^{2+} (except for those of Ce, Gd and Lu) have the electron configuration $4f^{(k)}[5s^25p^6]$. These special electron configurations give rise to characteristic narrow luminescence emission bands for REE ions with the configuration $4f^{(k-1)}f^{1*}$ through a $f^* \rightarrow f$ transition. The narrow luminescence emission band of the REE ion (trivalent or divalent) originates in the $4f$ subshell, which is partially shielded by $[5s^25p^6]$ electrons. Since interaction between the $4f$ electron and the crystal field is very weak (weaker than the spin-orbital interactions), the energy levels of the REE ions with a $4f^{(k-1)}f^{1*}$ configuration are not significantly influenced by the crystal fields. Therefore, for REE ions with a $4f^{(k-1)}f^{1*}$ configuration, the gross structure of the energy levels in the free REE ions is basically the same in the different host matrices.

REE ions with $f^* \rightarrow f$ transitions yield narrow luminescence peaks and show no Stokes shift. However, luminescence emission from REE ions can also take place in the $5d$ electron shell, which interacts strongly with the crystal field. Therefore, the luminescence emission from the transition $4f^{(k-1)}5d^{1*} \rightarrow 4f^{(k)}$ yields a broad band. Since for REE^{3+}, the energy levels of $4f^{(k-1)}5d^{1*}$ lie in the ultraviolet (UV) region, broad band transitions overlap with narrow transitions there. Also, since for REE^{2+}, the energy levels of $4f^{(k-1)}5d^{1*}$ are located in the visible region, the overlap with the dominant broad transition band may lead to difficulties in measuring the narrow peaks from REE^{2+} ions having an $f^* \rightarrow f$ transition in the visible region. In the region near infrared (IR), one may expect to find narrow transition bands from the REE^{2+} ions.

The effects of luminescence sensitization and quenching

Figure 3 is a schematic representation of what happens when the ion related luminescence transition energy is larger than, or close to, the energy band from the luminescence transition of a second ion. The energy released from the first ion does not show up in the final emission spectrum. Rather, it excites the second ion and thus enhances the luminescence emission from the second ion. This phenomenon is termed sensitization. The first ion is a sensitisor or coactivator, whereas the second one is an activator (Marfunin, 1979). Mn^{2+} is a typical activator, but when it coexists with REE^{3+} ions in a crystal, it can act as a sensitisor (coactivator). In a mineral, one REE ion can be a sensitisor to another REE ion.

A quenching effect represents another type of

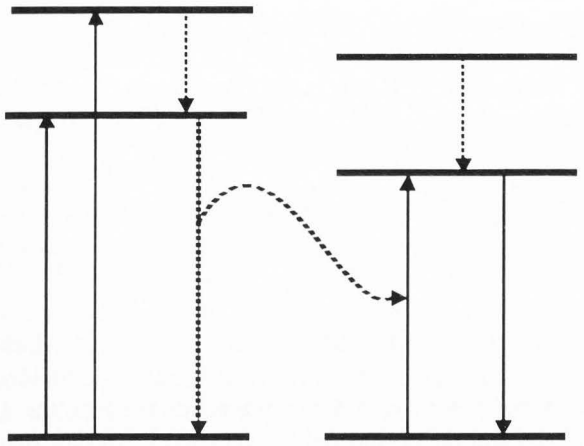

Figure 3. Sensitization of an ion (modified from Marfunin, 1979).

luminescence phenomenon. When an ion (quencher) is present in a matrix, the luminescence emission of another ion may be largely reduced or even disappear. In the process of sensitization, the second ion (the activator) is actually a quencher to the first ion (the sensitisor). The most notable quenchers are Fe^{2+}, Fe^{3+}, Co^{2+}, and Ni^{2+}. These ions have charge transfer bonds in their absorption spectra (Henderson and Imbusch, 1989) with peaks that lie in the UV region. The peaks are of significant intensity and are broad, their tails extending into the visible region and even approaching near IR (nIR) region (in the case of Fe^{3+}). If another ion related luminescence emission band is overlapped by such an absorption tail, the luminescence emission can be quenched.

Instrumentation of the Ionoluminescence System

The IL system employed here is one attached to the nuclear microprobe facility in Lund (Yang *et al.*, 1993). It is equipped with two monochromators. The first has a high wavelength resolution (typically set at 10 Å) but a low through-put for the acquisition of emission spectra. The operation range of the monochromator extends from UV to 10000 Å, with a grating of 1200 lines/mm. For spectroscopic analysis, it is usually set at an 800 μm slit width and a 5 Å/sec grating scan speed. The second is a filter monochromator with a wavelength tuneable range of 4000 Å to 7000 Å and a band-pass of about 100 Å to 200 Å. This monochromator, with its high through-put, is useful for IL imaging having a wavelength window. Two photomultiplier tubes (PMTs) are used for IL detection. One is of a Hamamatsu R585 type with a wavelength response region of 1600 Å to 6500 Å. Even when operated at room temperature, it has a very low dark current (as low as 1 photon count per second). The other is of a Hamamatsu R943-02 type, with a wide response region of wavelength 1600 Å to 9300 Å. If operated at room temperature, its dark current is as high as 10,000 cps, which is too noisy for good performance. Cooling it down to -30°C allows a very low noise level (one of about 50 cps) to be maintained, which is about the same order of light leakage as that present in the experimental set-up. Both PMTs are operated in the photon-counting mode.

The luminescence collection system consists of two lenses and a vacuum-sealing window, all of Optical Crown Glass®, which permits the transmission of luminescence light of wavelengths longer than 3500 Å. The response of the IL detection system extends from 3500 Å to 9300 Å. The spectroscopic data acquisition system consists of a Vax based data acquisition, display and processing system (Nuclear Data Inc., Genie ND9900) and a multichannel scaler (MCS) unit with multiple ports. A μVAXII computer is used as a host machine. Three ports of MCS data are recorded simultaneously. One port is used for the IL photon-counting signal; and the other two ports for the RBS signal and the digitized current signal for monitoring current variation in low current and high current, respectively. Usually, if there is a large variation in current, the IL data in a time sequence is normalized to the RBS data.

Interpretation of Luminescence by Combined Use of IL and PIXE

Most luminescence from minerals is of an extrinsic type, related to the activation, sensitization and quenching of different ion impurities which vary in abundance. Ions present at trace levels of parts per billion to parts per million (ppb to ppm) can suffice to cause the luminescence effects of activation, sensitization, or quenching. To understand the complexity of the luminescence phenomenon, a non-destructive, microbeam analytical method is needed so as to be able to identify and measure elements present at a very low concentration. PIXE is a well-established method with high sensitivity (ppm levels) for many elements.

Biogenic minerals

Biogenic carbonate is an important component in many sedimentary rocks; the chemical composition of the carbonates is commonly used by geochemists for characterizing sea water, diagenetic fluid compositions, and global bio-geochemical cycles, as well as for constraining stable isotope stratigraphy. CL in combination with electron microprobe analysis (EMPA) can be very

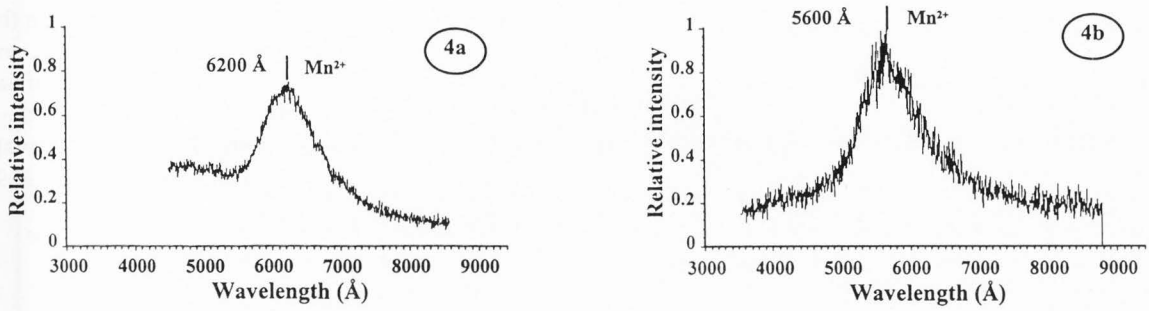

Figure 4. IL spectra in two sea shell samples with peak centers that differ, Mn^{2+} ions acting as luminescence activators; (**a**) shell with a calcite matrix showing a 6200 Å peak; (**b**) shell with an aragonite matrix showing a 5600 Å peak. Beam conditions: 2.5 MeV protons, beam size 100 μm, beam current 2.0 nA.

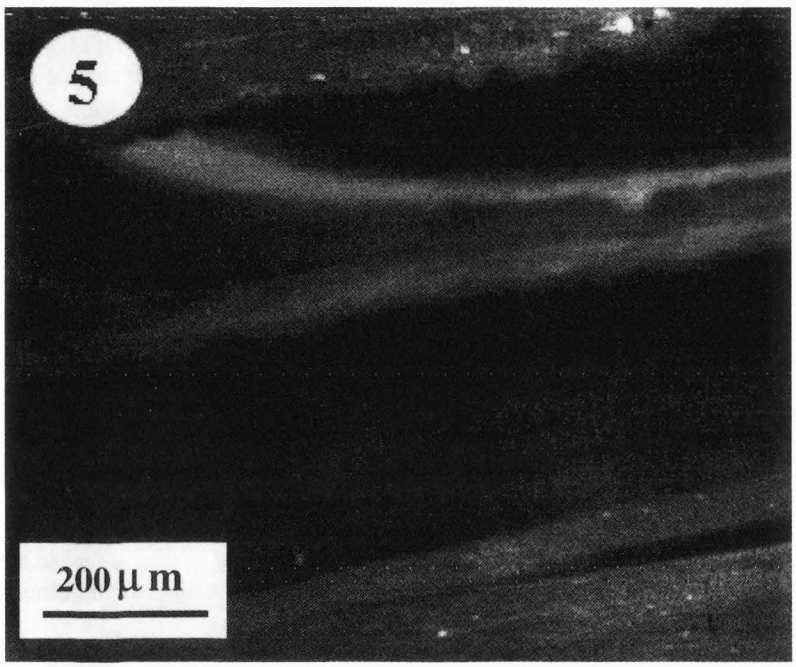

Figure 5. Hot cathodoluminescence photomicrograph of the sea shell with a calcite matrix. The orange-colored luminescence pattern under cathode ray (30 keV) excitation is very similar to that shown in IL and Mn maps in Figure 7.

useful for revealing chemical information in carbonates. Unfortunately, for many trace elements, the detection limits of EMPA are not satisfactory due to the ablation of carbonate samples. The combination of IL and PIXE offers a more sensitive alternative to CL/EMPA (by electrons).

Two types of recent sea shells, illustrating different ecological and mineralogical features, were investigated. The first shell, a bivalve (*Pecten maximus*), was found under shallow marine conditions (Bay of Brest, France; Barbin *et al.*, 1991); the second, a cephalopod (*Nautilus pompilius*, Barbin, 1992), a pelagic organism, came from Cebu (Philippines).

For CL investigation, a highly sensitive CL microscope (hot cathode; Ramseyer *et al.*, 1989) was employed. The experiments were carried out at an accelerating voltage of 30 kV and a beam current density of 0.4 mA/mm^2. The CL spectrum was recorded between 2000 and 9000 Å using a monochromator; the monochromator was set to 100 Å resolution and was linked to the CL microscope via a flexible optical fibre bundle. The CL detector was a PMT of the Hamamatsu R928 type. In order to reduce noise, multiple scans (ten measurements at each wavelength position) were integrated so as to obtain average results of good statistical quality for the spectrum.

The two sea shells display different colors in hot CL analysis: orange for the first and the greenish for the second. The IL spectrum from the first shell (*Pecten*) is shown in Figure 4a; Figure 5 shows the corresponding hot CL photomicrograph. The IL spectrum shows a broad distribution peaking at about 6200 Å. A PIXE

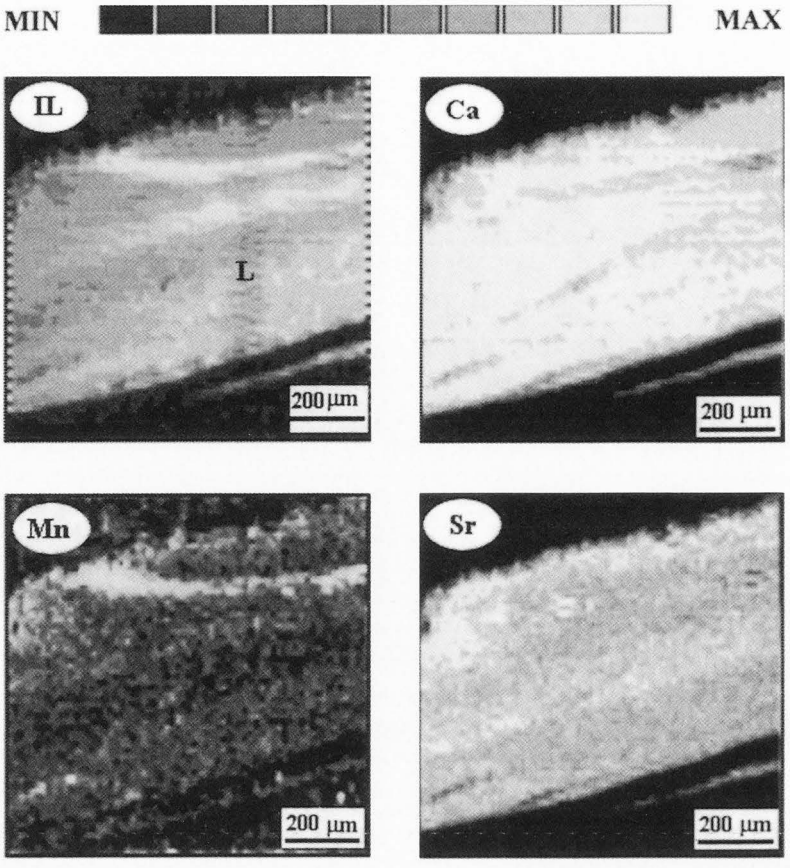

Figure 6. Mn distribution in the line scan denoted as "**L**" in **IL** map in Figure 7. Beam current of several nA; other beam conditions the same as in Figure 7. PIXE data evaluated by GEOPIXE (Ryan *et al.*, 1990).

analysis using a line scan and a very large beam current for good statistics was performed prior to the IL imaging experiment. The PIXE results from the line scan are shown in Figure 6. Figure 7 displays the IL and X-ray maps, the trace of the beam damage caused by PIXE analysis being visible as a "broken" line in the IL map. The pattern of IL is similar to that shown in the Mn X-ray map, which in turn is similar to that shown in the hot CL photomicrograph (Fig. 5). This indicates that the orange luminescence is a product of Mn^{2+} activation in the calcite matrix.

The second sea shell (of *Nautilus* type), which displays a greenish color in the hot CL photomicrograph, shows a similar color of light when it is excited by protons; its color center in the IL spectrum is at about 5600 Å (Fig. 4b). The main peak of the spectrum is similar to that obtained using CL (Barbin, 1992). The PIXE X-ray maps (not shown) confirmed that the Mn distribution pattern was virtually identical to that of CL.

The PIXE results support the view that the luminescence in both samples is activated by Mn^{2+}. Both sea shells consist of calcium carbonate, yet they show very different luminescence colors due to differences in their crystal structure.

As shown in Figure 2, the free Mn^{2+} energy levels are modified by the surrounding crystal field experienced by the Mn^{2+} ion: the luminescence transition occurring at the modified level $^4T_{1g}$. As is evident, a greater crystal field strength experienced by the Mn^{2+} results in a shorter transitional energy distance and in a larger Stokes shift, making the wavelength of the luminescence longer.

The shell displaying orange luminescence is calcite, whose structure is rhombohedral, and the shell showing green luminescence is aragonite (orthorhombic structure). In calcite, Mn^{2+} ions can occupy Ca^{2+} ion's site that is experiencing the crystal field generated by the closest anions in a less distorted octahedral symmetry. Whereas, in aragonite, the Mn^{2+} ions may occur in interstitial sites (Marshall, 1988), in which the crystal field experienced by the Mn^{2+} ions is much less than that of octahedral symmetry in calcite. The difference in crystal fields experienced by the activator ions leads to the difference in the luminescence colors they produce. From Figure 2b, one may conclude that the Mn^{2+} luminescence emission has a longer wavelength (orange) in calcite and a shorter wavelength (green) in aragonite.

The strength of the crystal field at the constitutional site of cation in three types of symmetry system has been discussed by Henderson and Imbusch (1989). The

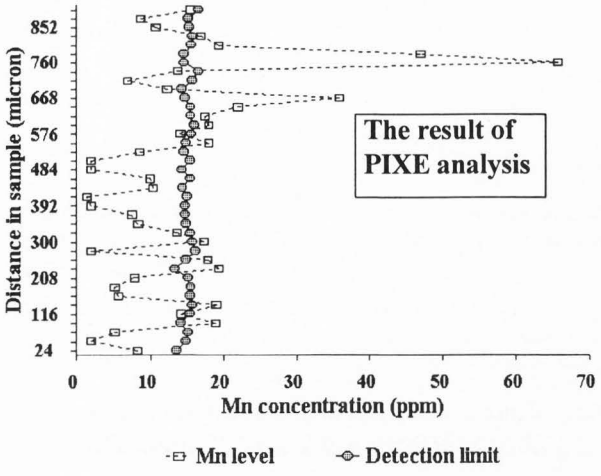

Figure 7. IL and elemental maps of the shell with a calcite matrix. The beam conditions: 2.5 MeV protons, beam current 100 pA, beam size 10 μm. In the IL map the noise signal from the sample supporter (glass) is subtracted using the **Ca** map in the figure as a mask. A weak broken line resulting from an earlier PIXE analysis is visible (indicated by "**L**").

---

relationship between the crystal field strength is formulated as $|Dq(\text{octahedral})| = 9/4\ |Dq(\text{tetrahedral})| = 9/8\ |Dq(\text{cubic})|$.

Characterization of zircon by IL and PIXE

Zircon is a common accessory mineral in many rocks, occurring as primary or inherited crystals in igneous rocks and as detrital and recrystallized grains in sedimentary rocks. It often contains trace amounts of REE, U and Th, and is thus used extensively in U-Pb geochronology (Heaman and Parrish, 1991). Zircon crystals have a tendency to show complicated growth histories in the form of oscillatory zones and overgrowths. In particular, the overgrowths tend to indicate a period of renewed crystal growth in response to changing chemistry in the fluid from which the mineral grows. When long periods of time have elapsed between periods of growth, this can result in radical differences in isotopic character between different regions of a single zircon crystal. The net effect of this is to make zircons "discordant," often resulting in erroneous determination of their age. It is important, therefore, that the growth history of zircon crystals be characterized by use of techniques that can distinguish between core and overgrowth features.

Inherited cores may be visible using an optical microscope, but examination by a scanning electron microscope (SEM) is generally required. An SEM compositional image [backscattered electron (BSE) mode] can reveal clear internal structures (in a sectioned and well-polished zircon grain), as does the CL image (Grauert

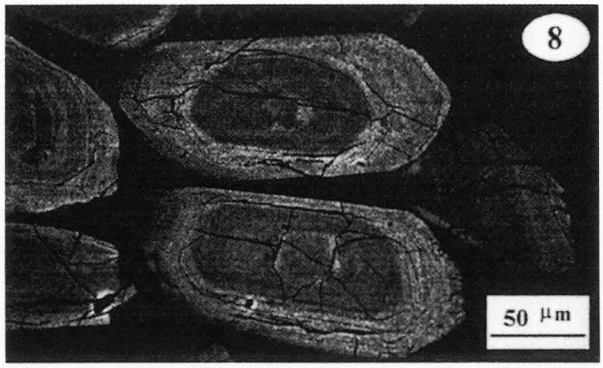

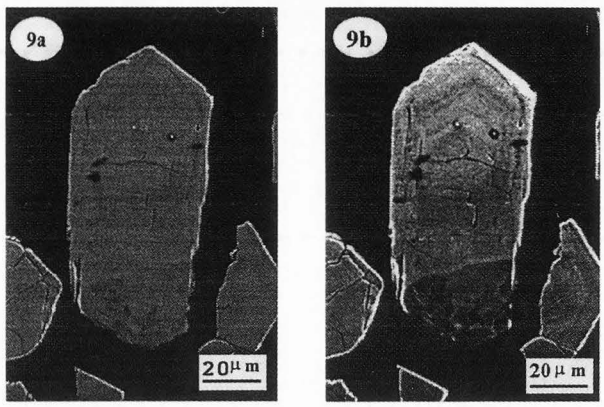

Figure 8. BSE image of well-polished zircon grains, obtained with a SEM. The cores are clearly revealed by the mean mass distribution pattern (light: high mass density, dark: low mass density). A 20 keV electron beam was employed.

Figure 9. Zircon grain no. 1 analysed by SEM: (**a**) secondary electron image (surface conditions); (**b**) BSE image (mean mass distribution). A core covered by new growth layers is not revealed here due to the short penetration range of the 20 keV electrons employed. The internal structure of the core in the same grain is clearly evident as in the IL and X-ray maps in Figure 10 that were produced by a 2.5 MeV proton beam.

---

and Wagner, 1975). The type of zircon included here is not suitable for single grain dating unless an ion microprobe is employed. The dark, slightly metamict core in Figure 8 may be older than the lighter zoned overgrowth. Figure 9 indicates that secondary electrons are of little use in determining the internal structure but that BSE can be used to show slight variations in composition. The zoning and overgrowth structure becomes more prominent when IL and PIXE X-ray imaging are employed, as shown in Figure 10.

A line scan across zircon is shown in Figure 11. It should be borne in mind that for X-ray imaging a considerable time is required to obtain good statistics,

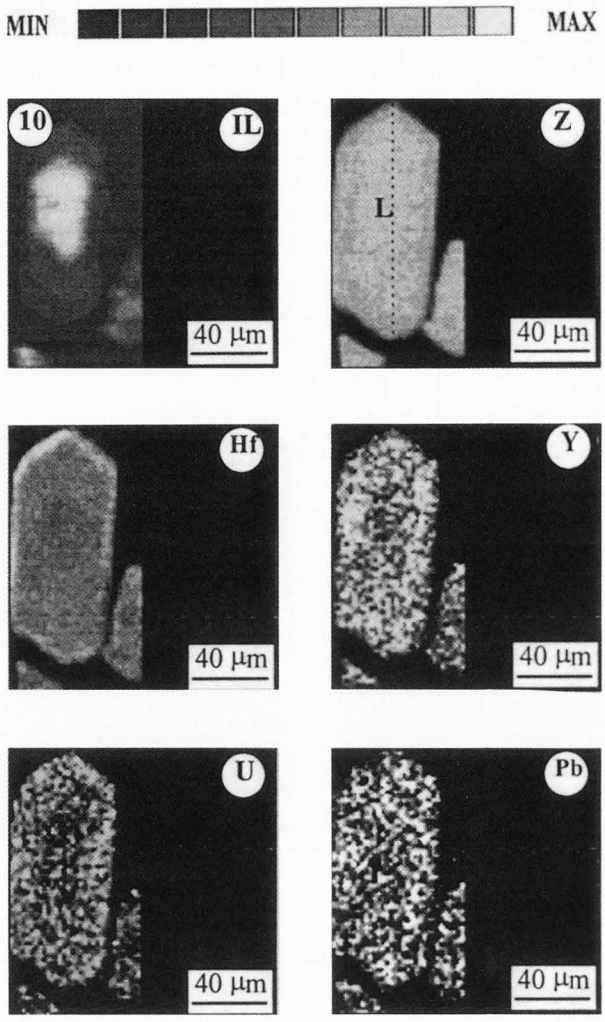

Figure 10. Zircon grain imaging. Beam conditions: 2.5 MeV protons, beam current of a few 10 pA for the **IL** map and of about 100 pA for the **Zr**, **Hf**, **Y**, **U**, and **Pb** elemental maps. Beam size about 5 μm. The same grain as observed by SEM in Figure 9, is analyzed. A line scan for PIXE analysis was performed at the location denoted by "**L**" in the **Zr** map. PIXE results of the line scan are shown in Figure 11.

---

whereas the high yield with IL, from such minerals as zircon, makes it possible to image such minerals within a few minutes.

In Figure 12 and 13, the results for a metamict zircon grain analyzed by both a SEM and a nuclear microprobe are shown. For the IL imaging, either proton or alpha beams, of the same energy level, are used. An alpha beam has a much shorter penetration range (about a 6 μm range with 2.5 MeV alpha particles) than a proton beam. A 20 keV electron beam typically has a penetration range of only 1-2 μm. An IL map obtained using alpha particles is shown in Figure 13a; it reveals

Figure 11. (**Facing page**) Elemental distribution in the line scan location denoted by "**L**" in the **Zr** map in Figure 10. Beam conditions: 2.5 MeV protons, beam current of several nA, 5 μm beam size.

---

sharper growth zones than does the IL map produced by protons in Figure 13b. For comparison purposes, PIXE X-ray maps (by protons) are shown in Figures 13c to 13f. Zr and Hf display antithetic variation, which is consistent with Hf substituting for Zr.

Characterization of the Oxidation State Through Combined Use of IL and PIXE

Figure 14 shows IL spectra from two different samples of plagioclase. Differences in the intensity of the Fe^{3+} peak are suggestive of different concentration levels of Fe^{3+} in the two samples. This may be due to: (i) product of the different absolute concentration levels of the element Fe; or (ii) differences in the abundance of oxygen at the time of mineral growth. Results with CL have suggested that the mineral oxidation state in plagioclase is determined by the luminescence peak area ratio of Fe^{3+} to Fe^{2+} (Mariano *et al.*, 1973; Marshall, 1988). There is some uncertainty regarding the existence of a Fe^{2+} luminescence peak. Even if there is a true peak, the broad peak that appears usually overlaps with a Mn^{2+} peak or other transition metal ion peaks, making the task of determination quite difficult. For REE, unlike REE^{3+}, the REE^{2+} related luminescence ($d^* \rightarrow f$ or $d^* \rightarrow d$ transition) peak is usually broad in the visible region and its peak center changeable. A similar difficulty is encountered in the analysis of the broad REE^{2+} peaks due to their sensitivity to the chemical surroundings. Since, in elemental analysis based on PIXE, only one IL peak from the trivalent ion may be needed, the problem can be resolved in a more reliable way. For example, if the ion X^{3+} in a mineral sample is under investigation, an PIXE X-ray spectrum can be obtained simultaneously with an IL spectrum in the same sample region.

For quantitatively combining the data of PIXE with that of IL, one has to consider the absorption problem. In the case of IL, ranging from visible to nIR and emitting from within a depth of few tens of μm, for most transparent minerals, the IL absorption usually can be ignored; otherwise, a factor of absorption must be taken into account, especially for the UV region. In PIXE, the X-ray attenuation effect is treated in the PIXE data evaluation software. In the case of the plagioclase study, the IL absorption is ignored and the X-ray absorption is treated in GEOPIXE code (Ryan *et al.*, 1990).

When quantifying a relationship between a specific

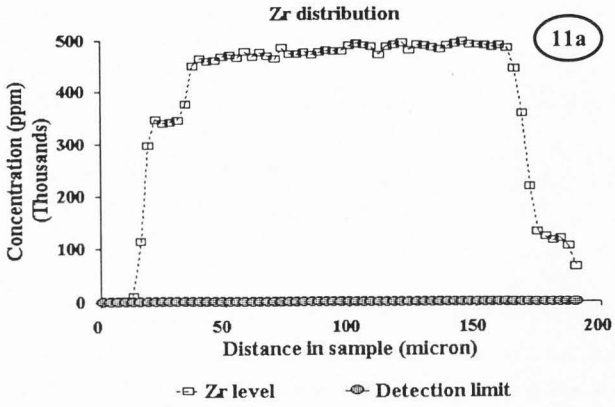
Zr distribution
11a
Concentration (ppm) (Thousands)
Distance in sample (micron)
Zr level
Detection limit

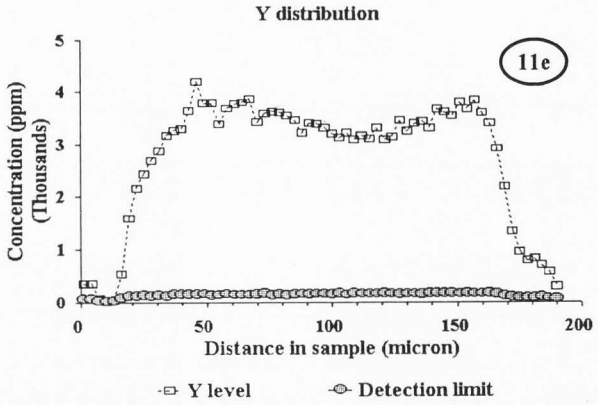
Y distribution
11e
Concentration (ppm) (Thousands)
Distance in sample (micron)
Y level
Detection limit

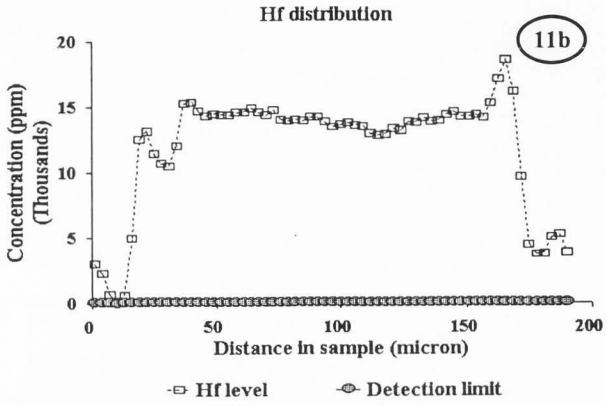
Hf distribution
11b
Concentration (ppm) (Thousands)
Distance in sample (micron)
Hf level
Detection limit

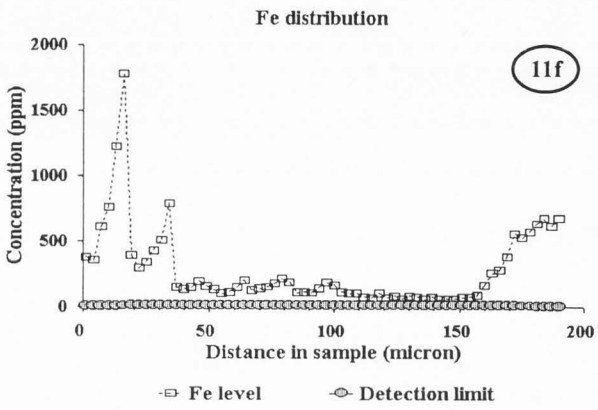
Fe distribution
11f
Concentration (ppm)
Distance in sample (micron)
Fe level
Detection limit

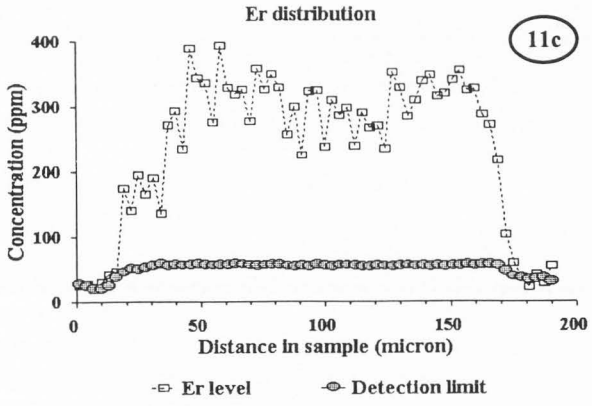
Er distribution
11c
Concentration (ppm)
Distance in sample (micron)
Er level
Detection limit

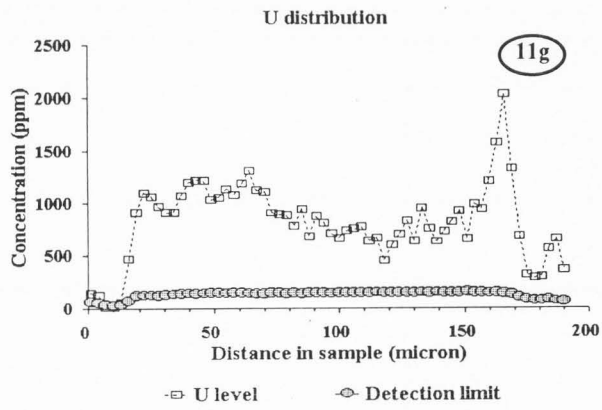
U distribution
11g
Concentration (ppm)
Distance in sample (micron)
U level
Detection limit

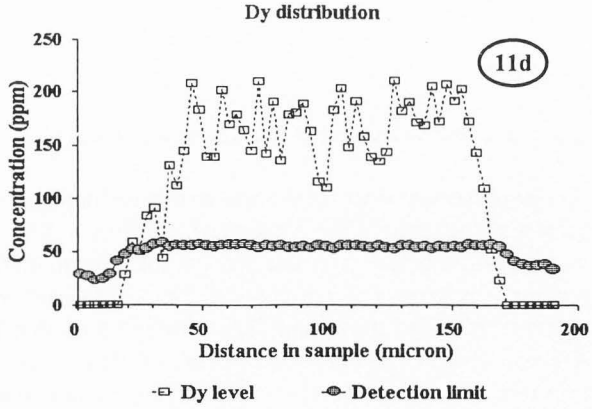
Dy distribution
11d
Concentration (ppm)
Distance in sample (micron)
Dy level
Detection limit

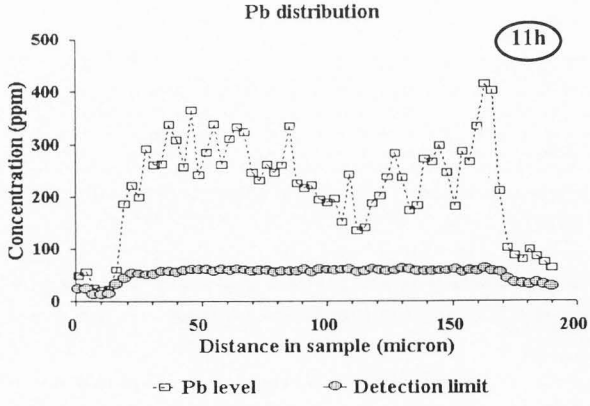
Pb distribution
11h
Concentration (ppm)
Distance in sample (micron)
Pb level
Detection limit

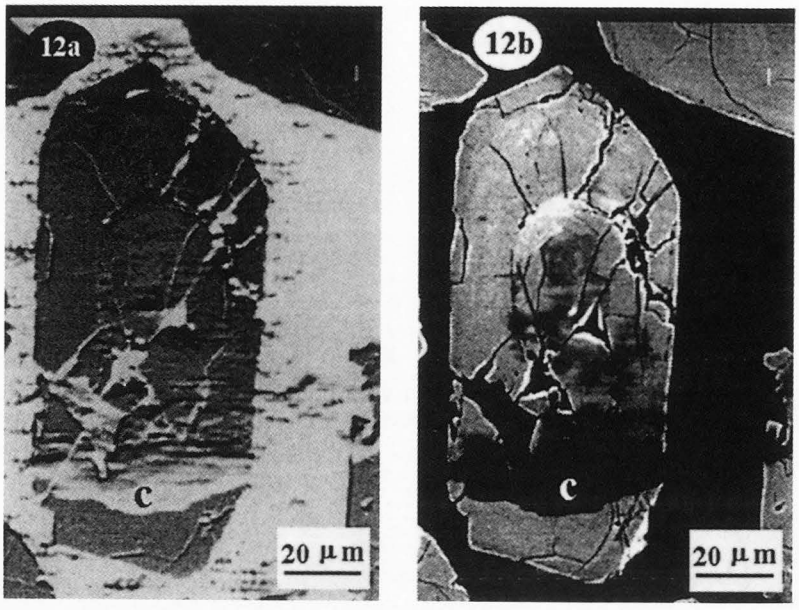

Figure 12. SEM images of zircon grain no. 2: (**a**) secondary electron image; (**b**) BSE image (light: high mass density, dark: low mass density). The **IL** and **X-ray** maps of the same grain are shown in Figure 13. Surface contamination is indicated by "**c**". A 20 keV electron beam was employed.

IL peak with the concentration of the related activator, one has to consider the influences from other impurity ions through the luminescence effects of coactivation or quenching. For a simplification of the first stage investigation, a synthetic mineral doped with one impurity may be a good solution. In order to obtain a condition for linear yield of IL, one still has to consider a proper dose for an activator. Marshall (1988) gives a range of maximum concentration as about 0.1-1% for a luminescence activator to be able to function in a mineral. If the concentration is too high, the activator ceases to function due to the self-quenching effect. Data of synthetic anorthite (Telfer and Walker, 1978) show a close linear relationship between Fe^{3+} related luminescence peak area and Fe^{3+} content in the concentration range of less than 0.2%.

For the simplified case, assuming the IL peak area $A_X{}^{3+}$ [IL counts] to be linearly proportional to the total X^{3+} content by the factor of IL efficiency, K (roughly constant if the experimental conditions remain unchanged and the samples belong to the same mineral), the percentage of X^{3+} in the total X element to be $P_X{}^{3+}$[%], and the total X element concentration to be C_X [%] (determined by PIXE), the following holds:

For sample S_1, the IL peak area of X^{3+} related luminescence is:

$$A_X{}^{3+}(S_1) = K \cdot P_X{}^{3+}(S_1) \cdot C_X(S_1)$$

and for sample S_2, involving the same type of the mineral, the X^{3+} related luminescence peak area is:

$$A_X{}^{3+}(S_2) = K \cdot P_X{}^{3+}(S_2) \cdot C_X(S_2)$$

hence,

$$P_X{}^{3+}(S_2) / P_X{}^{3+}(S_1) = [A_X{}^{3+}(S_2) / C_X(S_2)] / [A_X{}^{3+}(S_1) / C_X(S_1)]$$

A combination of IL and PIXE allows the oxidation state of an element in different samples of a given mineral to be determined. If the S_1 sample is a reference standard and S_2 represents different samples under investigation, the oxidation states of all the samples can be compared and analyzed in this way.

In a forthcoming paper, it will be shown that the IL results from plagioclase samples, which have very low and similar content of Mn^{2+} (a possible coactivator in plagioclase), are consistent with a geological knowledge of the oxidation conditions of the samples. However, a further proof of the technique is still required by comparing the IL results with those obtained using the other well-established techniques, e.g., the Mössbauer effect and UV photoemission spectroscopy applied to synthetic plagioclase to get information on chemical valence state of iron.

IL Spectroscopic Results of Some Minerals

Experiments with IL showed that beam damage affects the intensity but not the peak position. For IL acquisition, the beam current and the total accumulated charge were kept as low as possible, in most cases lower than that required in routine IBA. It was found that IL analysis should precede other forms of IBA so as to minimize the beam damage effect. The computerized

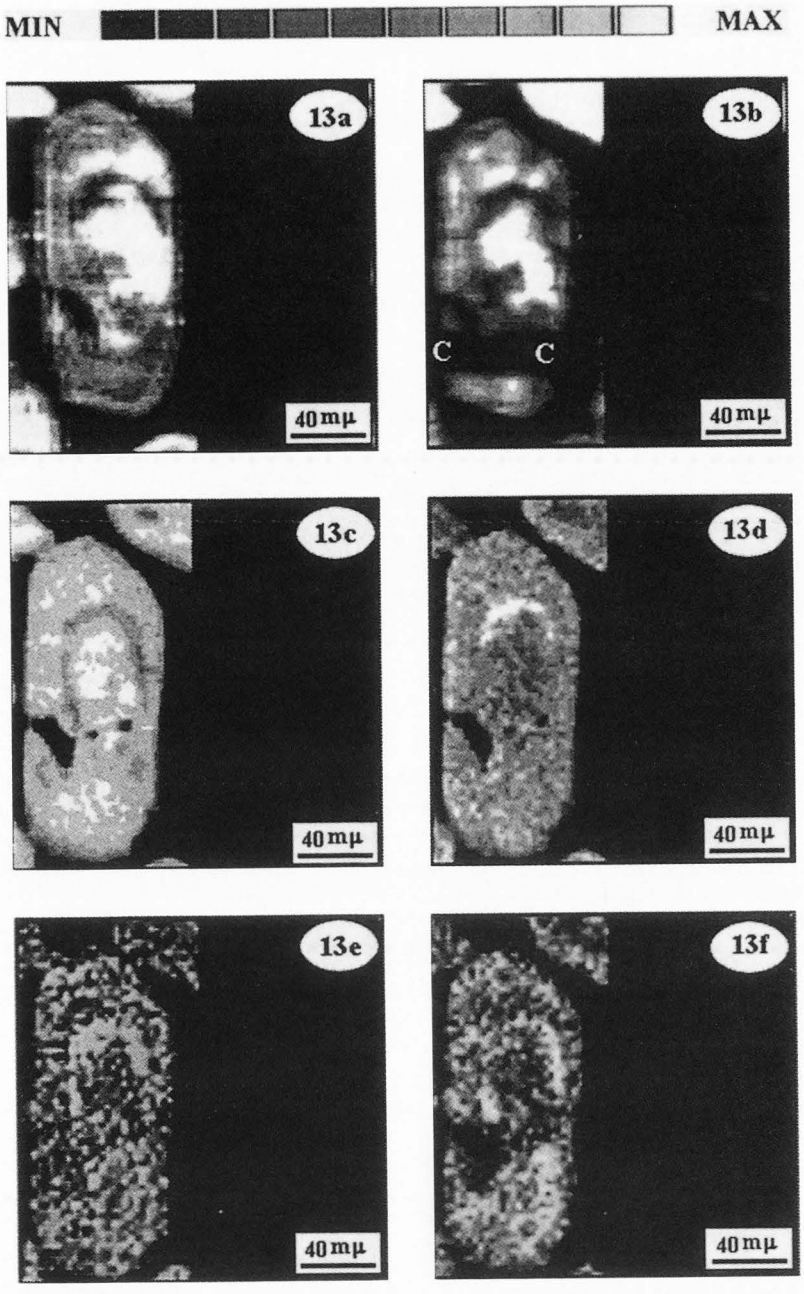

Figure 13. Zircon imaging of the same grain as in Figure 12. (**a**) IL with alpha beam excitation; (**b**) IL with proton beam, a surface contamination is indicated by "c" (**c**) zirconium; (**d**) hafnium; (**e**) uranium; and (**f**) yttrium. Beam conditions: 2.5 MeV alpha and beam current of less than 100 pA is for **IL** imaging in Figure 13a; protons are employed for other maps. 2.5 MeV proton, beam current of less than 100 pA for **IL** imaging in Figure 13b and of about 100 pA for **Zr**, **Hf**, **U** and **Y** elemental maps. Beam size about 5 μm.

system of the beam-position control in the nuclear microprobe enables IL and PIXE to be combined for analyzing the same vicinity of the sample.

In initial tests of the IL technique, a cooling stage was shown to be very useful; the cooling of a quartz crystal down to near liquid nitrogen temperature was shown to result in a significant increase in IL intensity. All the data presented here, however, are from experiments performed at room temperature.

IL activated by the transition metal ions: Mn^{2+}, Cr^{3+} and Fe^{3+}

$Mn^{2+}(3d^5)$ ion is a well known luminescence activator, the luminescence occurs due to the transition $^4T_1 \rightarrow {}^6A_1$. As shown in Figure 2, the free $Mn^{2+}(3d^5)$ energy level is modified by the crystal field. Differences in the strength of the crystal field experienced by the ion result in differences in luminescence color of Mn^{2+}. Hence, the luminescence of Mn^{2+} is a

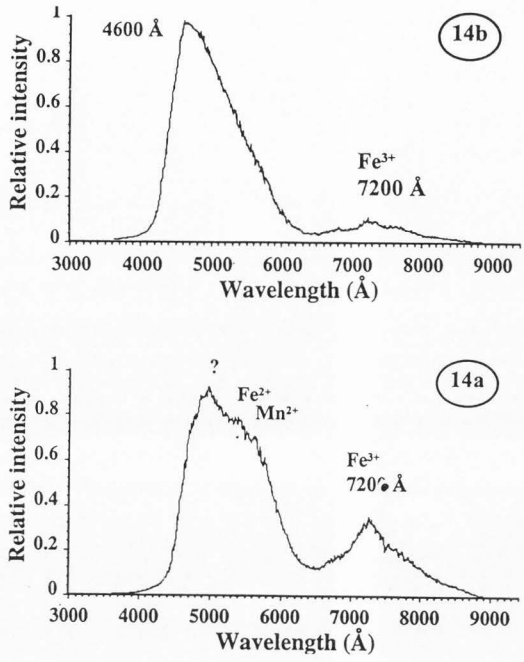

Figure 14. IL spectrum of plagioclase mineral. The two samples were tested under the same beam conditions: 1.5 MeV protons, 2.4 nA beam current, 100 μm beam size. The samples are from different locations. (**a**) Ti = 640 ppmw, Mn = 25 ppmw, Fe = 0.34%w; (**b**) Ti = 580 ppmw, Mn = 22 ppmw, Fe = 0.33%w.

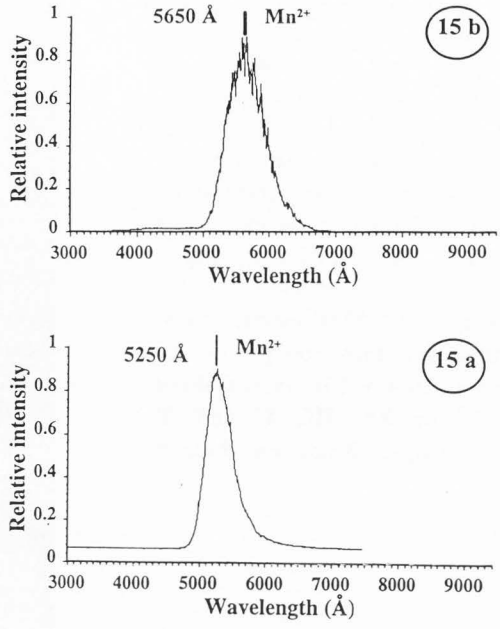

Figure 15. Mn^{2+} activated IL. (**a**) willemite mineral; Mn = 0.16%w; beam conditions: 2.5 MeV protons, 2.0 nA beam current, 20 μm focused beam size. (**b**) synthetic apatite; beam conditions: 2.5 MeV protons, 4.0 nA beam current, 150 μm beam size.

---

characteristic of the host matrix (Figs. 15a and 15b). However, since in the presence of REE ions, Mn^{2+} can also act as coactivator (sensitisor), it may not appear in the luminescence spectra of minerals containing large amounts of REE. If there are no REE ions, Mn^{2+} can be an efficient activator, as is evident in a spectrum of synthetic apatite (Fig. 15b).

$Cr^{3+}(3d^3)$ is another transition metal ion of great interest. Figure 16a shows a sharp line transition of $Cr^{3+}(3d^3)$ $^2E \rightarrow {}^4A_2$ for synthetic emerald, peaking at 6800 Å in the IL spectrum obtained. The broad IL distribution peaking at 7200 Å, is from the transition $^4T_2 \rightarrow {}^4A_2$. The Cr^{3+} sharp line is a well-known luminescence transition utilized in ruby laser, Cr^{3+} being in the Al_2O_3 trigonal system and peaking at about 6900 Å. The Cr^{3+} sharp line emission is due to a special feature of the $Cr^{3+}(3d^3)$ energy level in the crystal field (Fig. 16b). The crystal field strength of Cr^{3+} in emerald is very close to that in ruby. As shown in Figure 16b, the ^2E level is almost constant within a large range of the crystal field strength, Dq; in contrast, the $^4T_2$ level is much more sensitive to the strength of crystal field. For an impurity ion in a host, there is a statistical distribution of Dq, due to slight differences in the crystal environment and in the location of ions. Hence, the luminescence transition $^4T_2 \rightarrow {}^4A_2$ shows a very broad distribution. Since the sharp line has a very high quantum efficiency, a trace level of Cr^{3+} can be easily identified and detected (Holt, 1992).

$Fe^{3+}(3d^5)$ and $Fe^{2+}(3d^6)$ are usually luminescence quenchers, but they can also be activators in some cases (Mariano *et al.*, 1973). As discussed in the previous section and shown in Figure 14, Fe^{3+} and Fe^{2+} are activators in plagioclase. The ferric iron $Fe^{3+}(3d^5)$ is well-known as a luminescence activator both for CL (Mariano *et al.*, 1973; Marshall, 1988) and for PL (Marfunin, 1979; Henderson and Imbusch, 1989). The $Fe^{3+}(3d^5)$ peak (at about 7200 Å) is assigned to the transition $^4T_1(^4G) \rightarrow {}^6A_1(^4S)$.

REE^{3+} as a luminescence activator in different minerals

Synthetic calcite (REE dopants) Synthetic calcite crystals, doped with a single REE, either Sm (700 ppm), Eu (1144 ppm), Tb (750 ppm), or Dy (1300 ppm), were investigated using a 2.5 MeV proton beam. The materials were prepared at room temperature from aqueous solutions of calcium chloride and ammonium chloride. The REE dopants (Mason and Mariano, 1990) were added as chlorides. The IL spectra are shown in

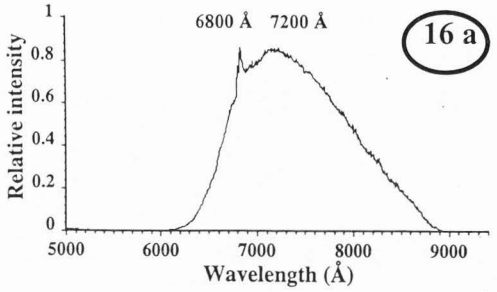

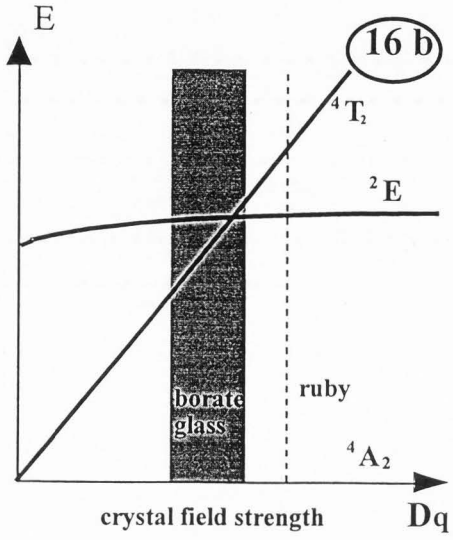

Figure 16. Cr^{3+} activated luminescence. (**a**) IL spectrum of emerald mineral; beam conditions: 2.5 MeV protons, 4.0 nA beam current, 100 μm beam size. (**b**) feature of Cr^{3+} energy levels in an octahedral crystal field (modified from Henderson and Imbusch, 1989).

Figures 17 to 20. Most IL peaks are identified with reference to PL data (Dieke and Crosswhite, 1963; Marfunin, 1979).

For Sm^{3+}, the following groups of peaks, in order of intensity from high to low, can be identified: $^4G_{5/2} \rightarrow {}^6H_{7/2}$ (6000 Å); $^4G_{5/2} \rightarrow {}^6H_{5/2}$ (5650 Å); $^4G_{5/2} \rightarrow {}^6H_{9/2}$ (6500 Å); $^4G_{5/2} \rightarrow {}^6H_{11/2}$ (7100 Å); and $^4G_{5/2} \rightarrow {}^6H_{13/2}$ (7800 Å).

For Eu^{3+}, the peaks are: $^5D_0 \rightarrow {}^7F_1$ (5900 Å); $^5D_0 \rightarrow {}^7F_2$ (6150 Å); $^5D_0 \rightarrow {}^7F_4$ (7000 Å); and $^5D_0 \rightarrow {}^7F_3$ (6500 Å).

For Tb^{3+}, the peaks are: $^5D_3 \rightarrow {}^7F_0$ (4900 Å); $^5D_4 \rightarrow {}^7F_5$ (5450 Å); and $^5D_4 \rightarrow {}^7F_3$ (6200 Å).

For Dy^{3+}, the peaks are: $^4F_{9/2} \rightarrow {}^6H_{13/2}$ (5750 Å); $^4F_{9/2} \rightarrow {}^6H_{15/2}$ (4800 Å); $4F_{9/2} \rightarrow 6H_{9/2}$ (7550 Å), $^4F_{9/2} \rightarrow {}^6H_{11/2}$ (6700 Å).

Zircon mineral Heavy REEs are compatible in zircon ($ZrSiO_4$), which has a tetragonal crystal structure.

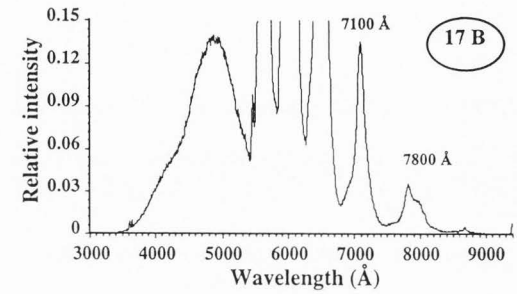

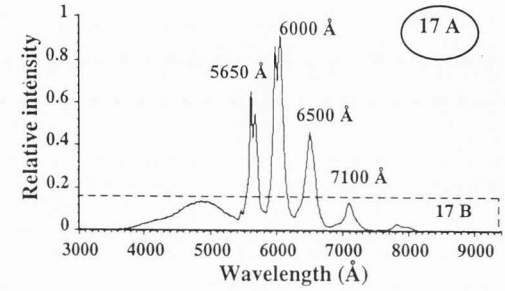

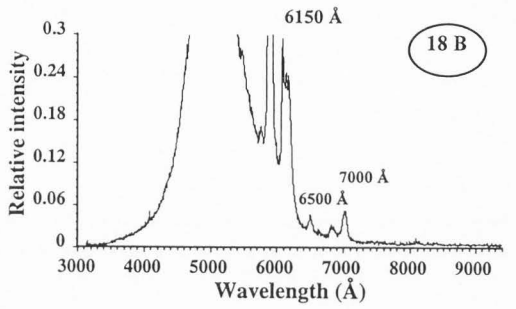

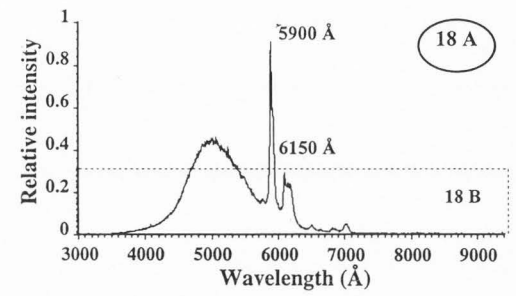

Figure 17. IL spectrum of synthetic calcite (Sm doped); Sm = 700 ppmw. Beam conditions: 2.5 MeV protons, 3.5 nA beam current, 10 μm beam size. PMT R943-02, grating scan speed 5 Å/sec.

Figure 18. IL spectrum of synthetic calcite (Eu doped); Eu = 1140 ppmw. Beam conditions: 2.5 MeV protons, 3.5 nA beam current, 10 μm beam size. PMT R943-02, grating scan speed 5 Å/sec.

However, since the trivalent Dy ion is a more efficient activator in zircon than are the other REE^{3+} ions, Dy^{3+} luminescence peaks are more easily detected. Figures

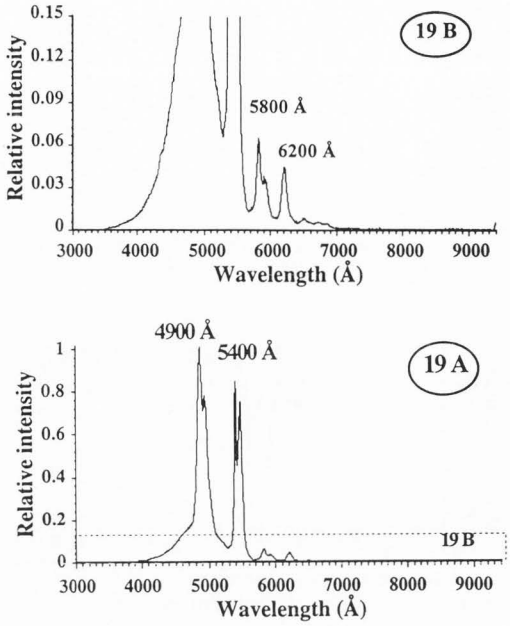

Figure 19. IL spectrum of synthetic calcite (Tb doped); Tb = 750 ppmw. Beam conditions: 2.5 MeV protons, 3.5 nA beam current, 10 μm beam size. PMT R943-02, grating scan speed 5 Å/sec.

21a and 21b show IL spectra from zircon crystals. While in Figure 21a, the Dy peak is clearly visible, in Figure 21b, the second the spectrum shows a broad distribution only. This may indicate the domination of sharp-line peaks of REE ions by the broad distribution originating either from the intrinsic luminescence emission or from an extrinsic emission activated by transition metal ions, or from both.

Apatite mineral Apatite [$Ca_5(PO_4)_3$(F, Cl, OH)] has a hexagonal crystal structure. It is a good host for different REE ions. The IL spectra of natural apatite samples from different sections containing REE ions are shown in Figures 22 and 23. With CL, it has been suggested that the main peak ratio of Sm^{3+} and Dy^{3+} can be used to obtain the ratio of the elemental contents of Sm to Dy, since the ions Sm^{3+} and Dy^{3+} in apatite occupy equivalent crystallographic sites and the strongest lines of the two ions have the same luminescence efficiency (Marshall, 1988). In present data, the main peak ratio of Sm^{3+} and Dy^{3+} appears to roughly agree with the PIXE data. For better quantitative IL results, a computer evaluation code for the IL data needs to be established and a better understanding of the luminescence physics concerning IL production in multi-impurity systems involved in quantifying the processes of luminescence activation, sensitization and quenching is required.

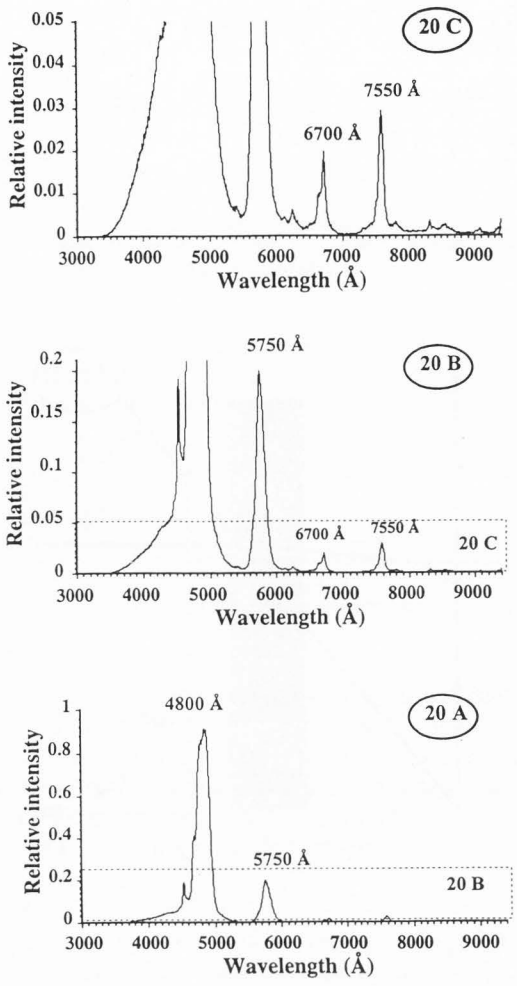

Figure 20. IL spectrum of synthetic calcite (Dy doped); Dy = 1300 ppmw. Beam conditions: 2.5 MeV protons, 3.5 nA beam current, 10 μm beam size. PMT R943-02, grating scan speed 5 Å/sec.

Titanite mineral Titanite [$CaTiSiO_4$(O,OH,F)] has a monoclinic structure. It is a common accessory mineral in igneous and metamorphic rocks. Just as with zircon, it can also be used for geological age-dating (Johansson and Johansson, 1993). The IL spectrum from a natural titanite mineral is displayed in Figure 24. Various REE ion peaks can be identified. A more detailed study of titanite will be presented in a forthcoming paper.

Beam Damage Effects in Ionoluminescence

The high efficiency of excitation energy conversion in IL is a major key for a limited beam damage effect in IL. For most luminescent minerals, there is usually no problem to obtain sufficient IL intensity with a limited

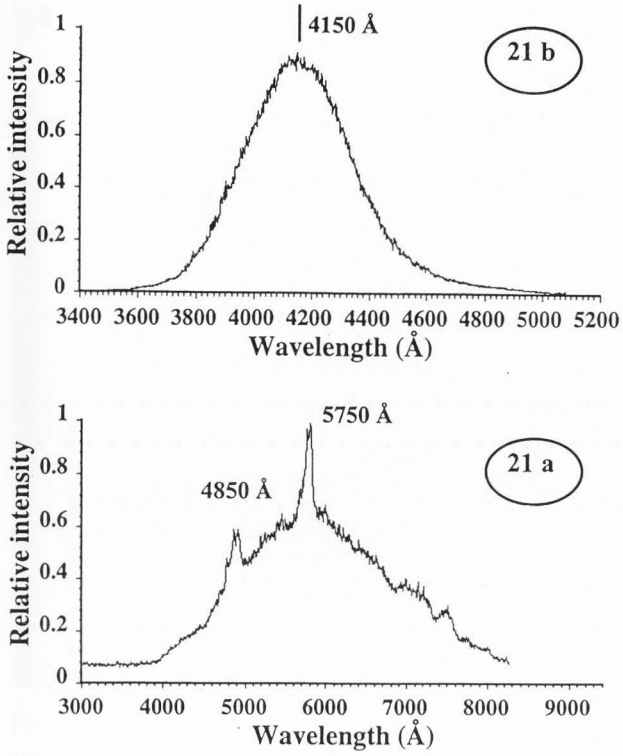

Figure 21. IL spectra of zircon mineral. (**a**) sharp peaks of Dy^{3+}; (**b**) broad peak is dominant, no REE sharp lines evident. Beam conditions: 2.5 MeV protons, a few nA beam current, beam size 20 μm. PMT R943-02, scan speed 5 Å/sec.

---

beam power (usually, beam intensity less than that demanded by the other IBA methods). The beam damage effect in IL is reflected in the IL intensity decrease under beam conditions typical for spectroscopy (2 nA current, 2.5 MeV protons). During data acquisition, the grating scan in a monochromator typically takes about 15 to 20 minutes to cover the wavelength region of interest. The longer wavelength regions suffer relatively more from beam damage effects than the shorter ones. The comparison of beam damage between IL and CL is discussed in a later section.

Beam damage monitored over time

A focused and fixed beam incident on a fresh area of apatite was used to study beam damage. Figure 25 shows photon counts of panchromatic IL plotted against time. The plot suggests that at the beginning of the experiment there was rapid IL decay when a fresh area was struck by the beam. The IL decay rate gradually decreased during the late stage of the run.

Beam damage in IL imaging

If panchromatic wavelength or a wide band-pass

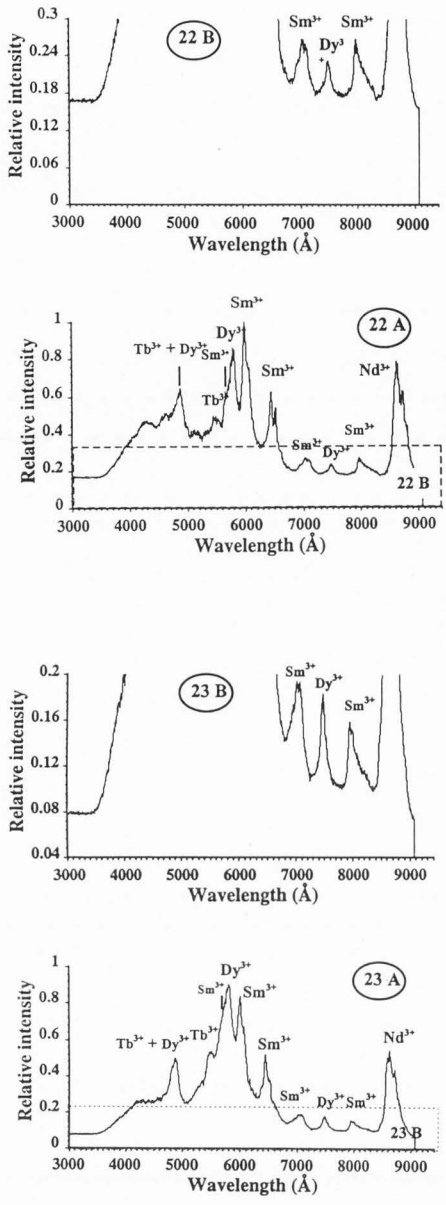

Figure 22. Apatite (section F) from Halland area in Sweden; Sm = 200 ppmw, Dy = 150 ppmw, Nd = 0.15%w, Er = 30 ppmw, Mn = 350 ppmw, and Fe = 0.2%w. Beam conditions: 2.2 MeV protons, 1.9 nA beam current, 20 μm beam size. PMT R943-02, scan speed 5 Å/sec.

Figure 23. Apatite (section D) from Halland area in Sweden; Sm = 178 ppmw, Dy = 255 ppmw, Nd = 0.10%w, Er = 100 ppmw, Mn = 800 ppmw, and Fe = 350 ppmw. Beam conditions: 2.2 MeV protons, 2.5 nA beam current, and 80 μm beam size. PMT R943-02, scan speed 5 Å/sec.

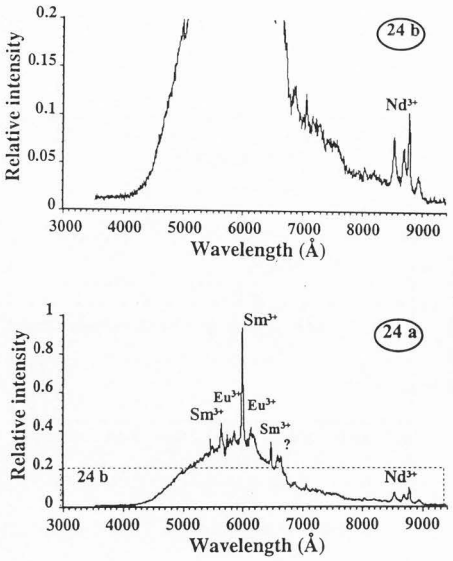

Figure 24. IL spectrum of titanite mineral. Various REE elements are presented in the sample. Beam conditions: 2.5 MeV protons, 3.0 nA beam current, 100 μm beam size. PMT R943-02, scan speed 5 Å/sec.

---

window are used for IL imaging, there is no visible beam damage in the imaging results, since the beam is moving and the beam current used for IL imaging is much less than that needed for IL spectroscopy. However, if the sample has previously been analysed by a focused and fixed beam using a large beam current, the beam damage is very noticeable, as shown in Figure 26. The dark spots in the IL image represent beam damage resulting from earlier PIXE analysis which used 1 μC of 2.5 MeV protons as the total dose at each spot and a beam size of 10 μm by 10 μm.

Comparison of Different Types of Luminescence

Although PL is a "traditional" luminescence technique, it nevertheless represents a modern and powerful method, particularly in conjunction with laser excitation. With a tuneable source, PL emission analysis can be easily combined with photon absorption or with excitation spectroscopy so as to reveal the detailed energy level structure of the material being studied. Hence, PL results usually have a concrete basis in optical spectroscopy that can be relied upon. Since the source power of PL is much less than that of CL or IL, the relative intensity of the peaks can be significantly different from that of the other two techniques. In addition, such secondary effects of CL and IL as internal charging,

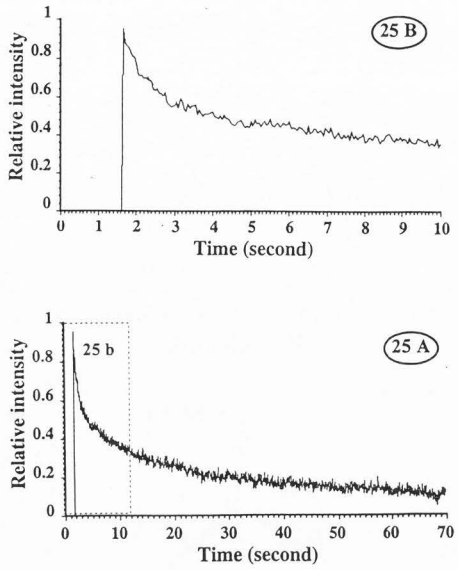

Figure 25. Beam damage in apatite as shown by IL decay; Beam conditions: 2.5 MeV protons, 20 μm beam size, beam density 5.0 x 10^{15} protons/sec/cm^2.

---

beam modification and damage may complicate the results they yield.

Spectroscopic IL results such as those presented here are usually referred to as PL data. However, although the peak position, and the position of the REE ion peaks in particular, agree well with those generally obtained using PL, the relative intensities of different peaks of IL differ greatly from those of PL. The differences are due mainly to the differences in excitation modes involved, and are due in part to the lack of calibration of the detection efficiency of the present IL system. CL, in turn, is widely used as an complementary imaging technique in SEM (Yacobi and Holt, 1990). If spectroscopic analysis with CL is combined with EMPA, information concerning the chemical microstructure of minerals can be obtained. Due to the low sensitivity of EMPA in trace element analysis, however, this does not permit the distribution of trace activators to be correlated with CL results. A combination of IL and PIXE resolves this problem, in that IL imaging can be carried out concurrently with PIXE analysis, the latter having detection limits for trace elements on the order of a few ppm.

In an inorganic solid, the penetration range of energetic protons having MeV energy is larger than 10 μm. Therefore, in IL the excitation volume extends from the surface to deep below the surface, the luminescence passing through a much greater volume before reaching the collection system than is the case of CL. The absorption effect, dependent on the optical properties of

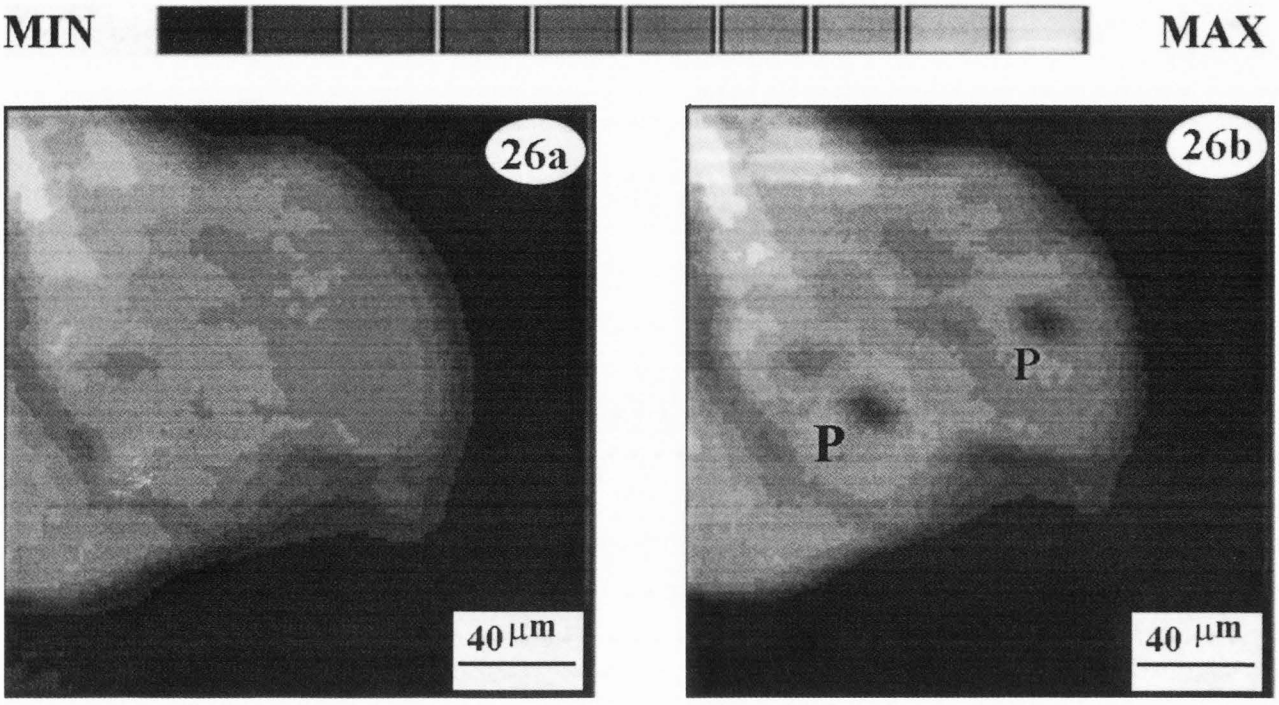

Figure 26. IL maps of an apatite grain; center of wavelength window for IL imaging at about 7100 Å. Beam conditions: 2.5 MeV protons, beam current of a few 10 pA, 5 μm beam size. (**a**) a fresh grain. (**b**) beam damage by PIXE spot analysis is indicated by "**p**"; the dose resulting in the damage spot is about 1 μC charge accumulation.

---

the mineral, can be more serious in IL than in CL. The relative intensity pattern of the peaks in IL may also differ greatly from that obtained with CL. In addition, IL can reveal information from a greater depth within a specimen than CL can.

The energy conversion efficiency in luminescence excitation is a major key for controlling beam damage. It is evident that protons in a few MeV energy range are highly efficient in luminescence excitation. For example, in the IL spectroscopic analysis of the minerals, the energy of the protons was generally about 2.5 MeV and the beam current 2 nA, resulting in a beam power of 5.0 x 10^{-3} [keV mA]; in the IL panchromatic imaging, a beam current of only a few tens of pA was needed for a quick image, leading to even lower beam power in the IL excitation. A meaningful comparison of the energy conversion efficiency between IL and CL will be dependent on the experimental data from systems whose detection efficiency is well calibrated.

There are a variety of effects involved in beam damage. For IL, most of the beam damage appears to result from the effect of secondary ions, such as secondary electrons, X-rays and recoiled atoms. The secondary ions produced can result in more serious beam damage in IL than in CL. The other beam damage effects in IL, such as heating-up and internal charging in a sample, tend to be rather slight compared with the ones that can occur in CL (Remond *et al.*, 1992). This is due partly to low beam current used with IL, particularly when panchromatic imaging is carried out, and partly to the much larger excitation volume for IL, making the energy deposition density much less. Damage from nuclear collisions with the primary incident protons is likewise very low in IL, again due to the low beam current.

As discussed by Remond *et al.* (1992), the internal charging in the sample introduces a secondary effect in CL results. In IL, the beam current is much less and the internal charging problem tends to be less serious. Also, since in IL the incident beam particles are positively charged, the type of effect may differ from that observed in CL.

Reducing beam damage effects can be achieved by maximizing IL detection efficiency. One such measure would be to increase the solid angle for IL collection. For example, an increase by a factor of 4 would be possible in the present system through use of an ellipsoidal mirror.

Discussion

Luminescence detection systems with a wavelength

response within the range of visible light are easy to set up. For most mineral materials, this region, only 3500 Å in width, seems too narrow to be of significant use. Also, it is crowded with broad distributions originating both from transition metal ions and from REE^{2+} ions through $d^* \rightarrow f$ or $d^* \rightarrow d$ transitions, and with narrow peaks originating from REE^{3+} through $f^* \rightarrow f$ transitions. If an effort were made to expand the detection region to include the UV region, various broad peaks from the $d^* \rightarrow f$ transition of REE^{3+} ions might still overlap other peaks. Thus, it might be more profitable to expand the detection region into the near infrared (nIR) or the IR region. The long wavelength region would presumably be relatively free of interference from broad distributions originating from transition metal ions and REE^{2+} ions through the $d^* \rightarrow f$ transition. In the nIR or the IR region, one could more easily investigate the narrow $f^* \rightarrow f$ transitions of REE^{2+} ions. Using the well-defined narrow peaking position from $f^* \rightarrow f$ transition in REE^{2+}, one could investigate the possible presence of certain REE^{2+} ions, such as those of $Sm^{2+}(4f^6)$, in minerals (Marfunin, 1979). Although from a geochemical point of view, it is unlikely that Sm^{2+} substitutes in natural minerals, it is possible from an optical spectroscopic point of view that in natural minerals some Sm^{2+} may coexist together with other REE^{3+} ions (Marfunin, 1979), probably at defect sites in the mineral structure. The electron configuration of most REE^{2+} ions (except those of Ce, Gd, and Tb) has the same structure as the next REE^{3+} in the Periodic Table. Since the electron configuration of $Sm^{2+}(4f^6)$ is identical with that of $Eu^{3+}(4f^6)$, the narrow $f^* \rightarrow f$ transition of $Sm^{2+}(4f^6)$ can be derived from $Eu^{3+}(4f^6)$ levels of $f^* \rightarrow f$ transition through lowering the energy levels of $Eu^{3+}(4f^6)$ by some 20% (Dieke and Crosswhite, 1963; Marfunin, 1979).

Using the IL data from the Eu- and Sm-doped synthetic calcite, one can identify a peak at 7000 Å for the Eu-doped calcite and a peak at 7100 Å for the Sm-doped calcite. The peak at 7000 Å obtained for the Eu-doped sample is probably the product of the $Eu^{3+}(4f^6)$ transition $^5D_0 \rightarrow {}^7F_4$. The $^5D_0 \rightarrow {}^7F_1$ transition of $Sm^{2+}(4f^6)$, corresponding to the strong $Sm^{2+}(4f^6)$ emission known in PL work on synthetic crystals (Wood and Kaiser, 1962; McClure and Kiss, 1963; Henderson and Imbusch, 1989), may also contribute to the IL peak at 7100 Å in the Sm-doped calcite sample. A similar small and relatively narrow peak in apatite at around 7100 Å may also come partially from $Sm^{2+}(4f^6)$.

A charge-coupled device (CCD) detector array system could help reduce beam damage by reducing the time needed for data collection, and could make it possible to carry out an IL study of the secondary effects of beam modification and beam damage in a reliable way. Sample cooling, as used in the case of CL and PL, would be likely to improve IL performance as well. Since energetic particles are used in IL, sharing the ion beam with such techniques as RBS-channelling could be useful. If a goniometer were used together with RBS-channelling, the crystal lattice could be selectively aligned to the beam direction, so that impurity ions in different lattice sites could be selectively analyzed by the beam. Thus, impurity ions at a interstitial or constitutional sites could be analysed in great detail. Crystal lattice damage could also be studied in this way.

Conclusions

Ionoluminescence appears to be highly useful in characterizing geological samples, especially when spectroscopic or microscopic methods within the framework of IL are combined with PIXE analysis. The combination of IL and PIXE can assist an understanding of extrinsic luminescence phenomenon through directly relating trace ions to the luminescence effects of activation, sensitization and quenching. Therefore, IL should provide a useful data base for the more effective utilization of luminescence in characterizing a variety of minerals.

Acknowledgements

We thank Dr. Lars Engström for his helpful comments and suggestions concerning the setting up of the IL spectrometer system and Kjell Håkansson for his help in producing various important components of the IL system. We also thank Dr. Roger Mason for use of the synthetic calcite crystals. Finally, we thank the Swedish Natural Science Research Council (NFR) for the continuous financial support of the present study.

References

Barbin V (1992). Fluctuation in shell composition in Nautilus (Cephalopoda, Mollusca): Evidence from cathodoluminescence. Lethaia **25**, 391-400.

Barbin V, Schein E, Roux M, Decrouez D, Ramseyer K (1991). Strie de croissance revelees par cathodoluminescence dans la coquille de Pecten maximus recent de la rade de Brest (Pectinidae, Bivalvia) [Growth bands revealed by cathodoluminescence in the recent Pecten maximus (Pectinidae, Bivalvia) from Brest bay]. Geobios **24**, 65-70.

Bettiol AA, Jamieson DN, Prawer S, Allen MG (1994). Ion beam induced luminescence from diamond and other crystals from a nuclear microprobe. Nuc. Instrum. Methods **B85**, 775-779.

Chu W-K, Mayer JW, Nicolet MA (1978). Backscattering Spectrometer. Academic Press, New York.

pp. 54-88.

Demortier G (1992). Twenty years of analysis of light elements at the LARN. Nuc. Instrum. Methods **B66**, 51-64.

Derham CJ, Geake DJE, Walker G (1964). Luminescence of Enstatite Achondrite meteorites. Nature **203**, 134-136.

Dieke GH, Crosswhite HM (1963). The spectra of the double and triply ionized rare earths. Applied Optics **2**, 675-686.

Faure G. (1986). Principles of Isotope Geology, Wiley and Sons. pp. 282-308.

Feldman LC, Picraux ST (1977). Ion Beam Handbook for Material Analysis. Academic Press, New York. pp. 10-45.

Grauert B, Wagner ME (1975). Age of the granulite-facies Metamorphism of the Wilmington Complex, Delaware-Pennsylvania Piedmont. Am. J. Sci. **275**, 683-691.

Heaman L, Parrish R (1991). U-Pb geochronology of accessory minerals. In: Short Course Handbook on Applications of Radiogenic Isotope Systems to Problems in Geology. Heaman L, Ludden JN (eds.). Mineralogical Association of Canada, Toronto. pp. 59-100.

Henderson B, Imbusch GF (1989). Optical Spectroscopy of Inorganic Solids. Clarendon Press, Oxford. pp. 68-77.

Holt DB (1992). New directions in scanning electron microscopy cathodoluminescence microcharacterization. Scanning Microsc. **6**, p.1-21.

Johansson SAE, Campbell JL (1988). PIXE: A Novel Technique for Elemental Analysis. Wiley, Chichester, UK. pp. 1-39.

Johansson L, Johansson A (1993). U-Pb age of titanite in the Mylonite Zone, southwestern Sweden. Geologiska Föreningens i Stockholm Förhandlingar. **115**, pt.1, P.1-7.

Kearsley A, Wright P (1988). Geological applications of scanning cathodoluminescence imaging. Euro. Microsc. Anal. **Sept**. 49-51.

Leverenz HW (1950). An Introduction to Luminescence of Solids. John Wiley, New York. pp. 312-321.

Malmqvist KG (1991). The nuclear microprobe: An instrument for trace element analysis and imaging. Euro. Microsc. Anal. **Nov**., 11-13.

Marfunin AS (1979). Spectroscopy, Luminescence and Radiation Centers in Minerals. Springer-Verlag, Berlin. pp. 188-211.

Mariano AN, Ito J, Ring PJ (1973). Cathodoluminescence of plagioclase feldspars. Geological Society of America (Boulder, Colorado), Abstracts with programs 5, 726.

Marshall DJ (1988). Cathodoluminescence of Geological Materials. Unmin Hyman, Boston. pp. 37-123.

Mason RA, Mariano AN (1990). Cathodoluminescence activation in manganese-bearing and rare earth-bearing synthetic calcites. Chem. Geol. **88**, 191-206.

McClure DS, Kiss Z (1963). Survey of the Spectra of the Divalent Rare-earth Ions in Cubic Crystals. J. Chem. Phys. **39**, 3251-3257.

Pringsheim P (1949). Fluorescence and Phosphorescence. Interscience Publishers, London. pp. 9-10.

Ramseyer K, Fischer J, Matter A, Eberhardt P, Geiss J (1989). A cathodoluminescence microscope for low intensity luminescence. J. Sedim. Petrol. **59**, 619-622.

Remond G, Cesbron F, Chapoulie R, Ohnenstetter D, Roques-Carmes C, Schvoerer M (1992). Cathodoluminescence applied to the microcharacterization of mineral materials: A present status in experimentation and interpretation. Scanning Microsc. **6**, 23-68.

Ryan CG (1993). The nuclear microprobe as a tool in geology and mineral exploration. Nuc. Instrum. Methods **B77**, 381-398.

Ryan CG, Cousens DR, Sie SH, Griffin WL, Suter GF, Clayton E (1990). Quantitative PIXE microanalysis of geological material using the CSIRO Proton Microprobe. Nuc. Instrum. Methods **B47**, 55-71.

Swietlicki E, Larsson NP-O, Yang C (1993). Multivariate statistical processing elemental maps from nuclear microprobe. Nuc. Instrum. Methods **B77**, 195-202.

Telfer DJ, Walker G (1978). Ligand field bands of Mn^{2+} and Fe^{3+} luminescence centers and their site occupancy in plagioclase feldspars. Mod. Geol. **6**, 199-210.

Wood DL, Kaiser W (1962). Absorption and Fluorescence of Sm^{2+} in CaF_2, SrF_2 and BaF_2. Phys. Rev. **126**, 2079-2088.

Yacobi BG, Holt DB (1990). Cathodoluminescence Microscopy of Inorganic Solids. Plenum Press, New York. pp. 21-26.

Yang C, Larsson NP-O, Swietlicki E, Malmqvist KG, Jamieson DN, Ryan CG (1993). Imaging with Ionoluminescence (IL) in a Nuclear Microprobe. Nuc. Instrum. Methods **B77**, 188-194.

Yang C, Homman NP-O, Johansson L, Malmqvist KG (1994). Microcharacterizing zircon mineral grain by ionoluminescence combined with PIXE. Nuc. Instrum. Methods **B85**, 808-814.

Discussion with Reviewers

S.H. Sie: Do the authors see any evidence of self-annealing effects in the IL measurements, especially at low beam intensities?

Authors: We see something likely to be an annealing effect in panchromatic-IL data at a very low beam inten-

sity. We notice IL yield enhanced by a small beam dose in IL imaging and IL yield monitored in time-sequence, but we are not sure if it is a self-annealing effect or an effect introduced by a beam damage. Unfortunately, we cannot acquire IL spectroscopic data at so low beam current (about 10 pA) under the condition of the present system. Generally, a large beam dose results in a continuous decay of IL intensity. We think that there is a competing process of annealing undergoing along with beam damage when energetic particles impinge into crystal. If other well established and non-destructive techniques can be applied *in situ* to analyze the change introduced by the ion beam, reliable results may be reached.

G. Remond: The authors indicate that the energy levels of the REE ions are not significantly influenced by the crystal fields. Cathodoluminescence studies have reported that small shifts in the peak position of the narrow CL emission lines occur as a function of the REE bearing minerals. Are these peak shifts also observable with ionoluminescence?

Authors: Yes, we did repeatedly observe REE^{3+} narrow peak shift in different minerals. Actually, we even observed very fine structure in peak splitting that is also dependent on crystal matrix. Recently, we carefully tested a synthetic zircon (Dy doped) under a condition of high wavelength resolution (about 2 Å) and observed that there are about 6 peaks around 4850 Å and 8 peaks around 5750 Å. We have not systematically studied these yet.

S.H. Sie: Can the authors comment on the conductivity of the samples versus loss or otherwise of the IL intensity?

Authors: As mentioned above, we observed an enhancement of an IL intensity by a low dose of ion beam. However, a large dose integration of the ion beam usually results in permanent beam damage indicated by a continuous decay of the IL intensity. The corresponding changes in the conductivity at respectively low and high dose may be observed in semiconductors. Unfortunately, at the present state, we do not have any experimental data on conductivity measurement that can be related to IL. The material we have analyzed most by IL is insulation crystal with a wide band-gap. The samples are usually carbon-coated for eliminating the charging effect introduced by an incident ion beam.

S.H. Sie: Did the authors try to determine the threshold of radiation loss of IL intensity using defocused beam?

Authors: No, we did not. The threshold might be dependent firstly on ion beam conditions, and secondly on properties of samples. The different color centers may differ in sensitivity to their chemical surroundings which can be modified by the incident ion beam. It would be very interesting to see the different responses to beam modification or damage for different color centers in a variety of minerals.